Nanoscale

Accepted Manuscript

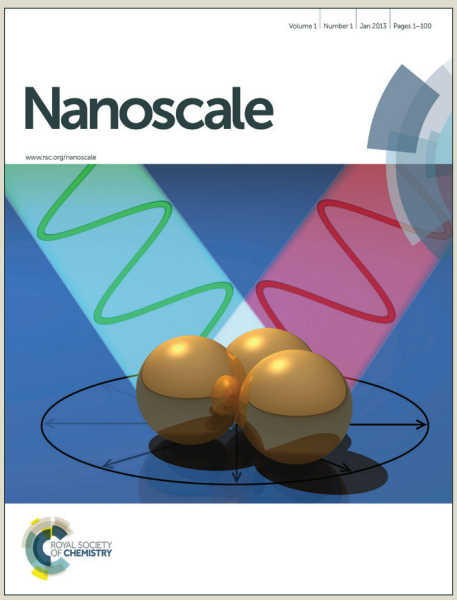

ROYAL SOCIETY OF CHEMISTRY

www.rsc.org/nanoscale

Cite this: DOI: 10.1039/c0xx00000x

www.rsc.org/xxxxxx

Communication

Improved Functionality of Graphene and Carbon Nanotube Hybrid Foam Architecture by UV-ozone Treatment

Wei Wang,[a,b] Isaac Ruiz,[b] Ilkeun Lee,[c] Francisco Zaera,[c] Mihrimah Ozkan*[b] and Cengiz S. Ozkan*[a,b]

Received (in XXX, XXX) Xth XXXXXXXXX 20XX, Accepted Xth XXXXXXXXX 20XX

DOI: 10.1039/b000000x

Optimization of the electrode/electrolyte double-layer interface is a key factor for improving electrode performance of aqueous electrolyte based supercapacitors (SCs). Here, we report the improved functionality of carbon materials via a non-invasive, high-throughput, and inexpensive UV generated ozone (UV-ozone) treatment. This process allows precise tuning of the graphene and carbon nanotube hybrid foam (GM) transitionally from ultrahydrophobic to hydrophilic within 60 sec. The continuous tuning of surface energy can be controlled by simply varying the UV-ozone exposure time, while the ozone-oxidized carbon nanostructure maintains its integrity. Symmetric SCs based on the UV-ozone treated GM foam demonstrated enhanced rate performance. This technique can be readily applied to other CVD-grown carbonaceous materials by taking advantage of its ease of processing, low cost, scalability, and controllability.

Introduction

Supercapacitors (SC) are a promising energy storage device because they can store and deliver charge at a very high rate (within seconds). With the increasing demand for high power density energy storage devices, SC research has exploded in the past few years. Since the storage mechanism for electrochemical capacitors primarily consists of surface storage, nanostructured synthetic carbon materials have attracted tremendous attention due to their unique combination of chemical and physical properties including high conductivity, large surface area, good corrosion resistance, controlled pore structure, processability, compatibility in composite materials, and relatively low cost.[1-7] Although pseudocapacitors employing transition metal oxides[8-10] and conducting polymers, etc.[11, 12] have been increasingly studied, carbon materials based supercapcitors remain the most extensively studied and least expensive applicable choice for practical applications. Finding new electrode materials and optimization of available electrode materials are the primary consideration for improving the specific capacitance of SCs. Various nanostructured synthetic carbon materials such as carbon spheres/onions,[2, 3] carbon nanofiber/nanotubes,[13, 14] activated carbon,[15] template derivered carbon,[16] carbide derived carbon,[17] and more recently graphene based materials[6, 18, 19] have been investigated comprehensively for SC applications. Pioneer investigations on effects of pore size and surface area suggest the performance of SCs can be improved by maxmizing the eletrolyte accessible surface area.[20, 21] Furthemore, chemical vapor depostion (CVD) grown synthetic carbon nanostructures have been verified to be an effective, facile, binder-free technique for the prepration of SC electrodes with high electrochemical performances.[13, 22-28] The seamless connection between active material and current collector facilitates charge transfer within the electrode which enhances the rate performance and stability dramatically.

In addition, we believe that optimization of the electrode/electrolyte double-layer interface is another key factor to improve the electrode performance of SCs. This may especially be significant for aqueous electrolyte based SCs, which are safer and easier to be fabricated. Better electrode-electrolyte interface is critical to extract full performance out of the electrode system. Surface functionalization techniques including high temperature H_2O etching, plasma treatment, chemical functionalization and activation, etc have been verified to be effective in enhancing the electrode/electrolyte interface for carbon nanostructures.[22, 25] However, all of these reported approaches require harsh conditions such as high temperature, low pressure, complicated processing, long processing time, damage to electrode materials, etc.

In this work, we report the improved functionality of carbon materials via a non-invasive high-throughput inexpensive UV generated ozone (UV-ozone) treatment. We take 3D graphene and CNT hybrid foam nanostructure (GM) as an example to systematically study the effects and mechanisms of improved functionality. Notably, we observed that the UV-ozone treatment allows precise tuning of the GM foam transitionally from hydrophobic to hydrophilic within 60 sec, which suggests a faster and superior approach when compared with previously reported treatment method using potassium hydroxide (KOH).[26] Contact-angle measurement, Raman, X-Ray photoelectron spectroscopy (XPS), infrared spectroscopy, and transmission electron

microscopy (TEM) were performed to characterize the structural change of the UV-ozone treated sample. Symmetric SCs have been fabricated based on the UV-ozone treated GM foam. The results suggest this UV-ozone treatment is a very promising dry process approach to tailor carbonaceous electrodes for improved supercapacitor rate performance, durability, and stability.

Experimental Section

Materials synthesis

Graphene and CNTs foam and pillared graphene nanostructure are grown via a chemical vapor deposition (CVD) process on conductive substrates which are nickel foam and copper foil, respectively in this work.[26, 29] The conductive substrates are pre-annealed to release the residue stress and washed to remove contaminants. Next, 1-5 nm iron catalysts are deposited on conductive substrates by e-beam evaporation (Temescal, BJD-1800). The treated Ni foam is heated to 750 °C, and hydrocarbon gas is introduced to trigger and continue the growth of graphene and CNTs synchronously on the nickel foam frame. The UV Ozone treatment is carried out in an instrument equipped with both its original 254 nm radiation lamp and an additional 185 nm radiation source. The average power of the UV is set to 30000 μW cm^{-2}.

Materials characterization

The morphology of material is investigated using scanning electron microscopy (SEM; leo-supra, 1550) and transmission electron microscopy (TEM; Philips, CM300) with a LaB_6 cathode operated at 300 KV. The TEM samples were prepared by ultrasonicating a small piece of sample in ethanol to form a dispersed solution and then coating the dispersed solution onto carbon film coated TEM grid by simply dropping. A Renishaw DXR Raman spectroscopy system with a 532 nm laser (8mW excitation power, 100x objective lens) source is used to characterize the UV Ozone treated GM foam. Kruss Easy drop (FM 40) technique is employed to measure the contact angle of the grapheme films. The FTIR study is performed by using Bruker Equinox 55 FTIR with a MCT detector. X-ray photoelectron spectroscopy (XPS) characterization was carried out by using a Kratos AXIS ULTRADLD XPS system equipped with an Al K monochromatic X-ray source and a 165-mm electron energy hemispherical analyzer. The vacuum pressure was kept below 3×10^{-9} torr, and a charge neutralizer was used during the data acquisition.

Fabrication and characterization of SCs

A symmetrically packaged SC configuration is employed for the electrochemical measurements, where the two working electrodes are assembled into a sandwich structure with a porous membrane functions as a separator in-between. An aqueous electrolyte (2 M Li_2SO_4) is used in this work. Cyclic voltammetry (CV), chronopotentiometry (charge-discharge (CD)), and electrochemical impedance spectroscopy (EIS) were conducted to evaluate the performance of the SCs. Potentiostatic EIS measurements were performed between 0.1Hz and 1MHz with amplitude of 10 mV. Specific capacitance C_s values are calculated from the charge-discharge curves via equation $C_s=\int IdV/(m\Delta VS)$, Where m is the mass of active electrode materials which is the loading of carbon nanostructures on nickel foam in this work, $\int IdV$ is the enclosed area of the CV curve, ΔV is the operational voltage window and S is the scan rate.

Results and Discussion

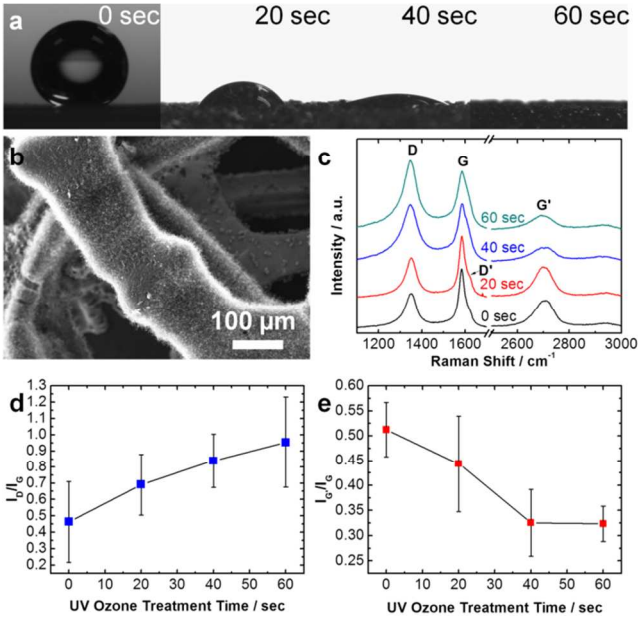

Fig. 1 (a) Contact angle measurements of the CVD grown GM foam over time upon exposure to ozone at room temperature. (b) SEM image of the GM foam. (c) Raman spectra of GM foam with a UV-ozone treatment time of 0 sec, 20 sec, 40 sec, and 60 sec, respectively. (d) ID/IG and (e) IG'/IG with exposure time. All Raman spectra are collected on nickel foam substrate. Laser excitation: 532 nm.

GM foam samples were treated with UV-ozone for 0 sec, 20 sec, 40 sec, and 60 sec. Contact angle measurements of the UV-ozone treated GM foam samples reveal that wettability of the GM samples are enhanced with increased treatment time (Fig. 1a). Through this dry method, the 3D GM foam change from completely hydrophobic to hydrophilic within 60 seconds, which is much faster when compared with previously studied wet chemical treatment methods.[25, 26] The GM foam is grown via ambient pressure CVD process. The as-grown GM foam demonstrates a hierarchical nature with very good coverage of CNTs on the graphene covered nickel backbone (Fig. 1b). To understand the mechanism of the surface energy change, Raman spectroscopy was conducted to investigate the structural changes in GM foam as a function of UV-ozone exposure time (Fig. 1c). Raman spectra collected from pristine and UV-ozone treated GM samples are in good agreement with the multi-walled carbon nanotube (MWCNT) Raman spectra, which shows the presence of the D band centered around 1380 cm^{-1}, and G band centered around 1570 cm^{-1}.[30] The G' band centered around 2700 cm^{-1} is a single peak, which is similar to that of graphene. The D band is associated with the defects of the CNTs. All spectra in Fig. 1c are normalized based on the G band. It is observed that the intensity of the D band increases with the prolonging of UV-ozone

exposure time. With the increase of UV-ozone exposure time, the D to G peak intensity ratio (I_D/I_G) increases from ~ 0.45 to ~0.95 within 40 sec and tends to stabilize ~1.0 afterwards (Fig. 1d). Fig. 1e shows the G' to G peak intensity ratio ($I_{G'}/I_G$) decreases from ~ 0.52 to ~0.32 in 40 seconds. The increase in I_D/I_G and the decrease in $I_{G'}/I_G$ suggest a structural change via doping which is generally activated by local basal distortion with the formation of defect-like sp^3 bonds in carbon materials.[31] Moreover, in Fig. 1c, a minor D' band at ~1620 cm^{-1} is observed after 20 sec UV-ozone treatment. The D' band tends to merge together with G band with longer treatment time.

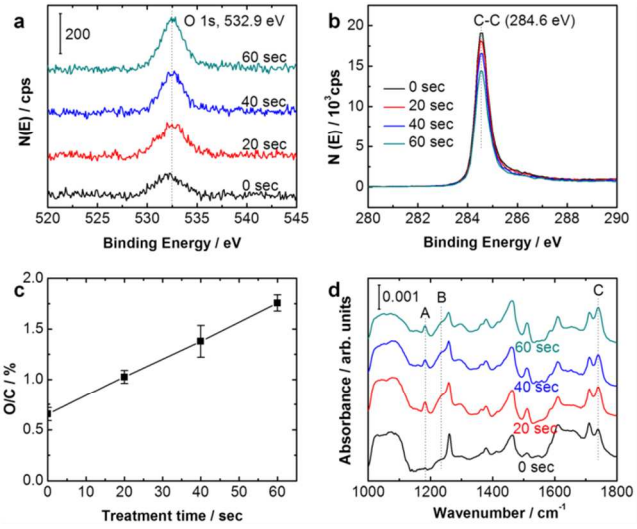

Fig. 2 (a) O 1s spectra and (b) C 1s of GM foam before and after (20, 40, 60 sec) treatment. (c) Relative atomic ratio of O to C as function of UV/O3 treatment time. (d) Attenuated total reflection infrared (ATR-IR) spectra of GM foam before and after treatment.

X-ray photoelectron spectroscopy (XPS) was performed to further elucidate the effects of UV-ozone exposure on the GM foam (Fig. S1). XPS experiments were conducted directly on GM foams with a nickel backbone to eliminate contamination from etching and transfer processes. Upon exposure to UV-ozone treatment, the O 1s peak shifts slightly, to a binding energy value of ~ 532.9 eV, and it becomes sharper (Fig. 2a). Increasing the exposure time from 0 sec to 60 sec increases the intensity of the O 1s XPS peak. The intensity of the C 1s peak (~284.6 eV), on the other hand, drops with increasing UV/O_3 exposure time. These observations suggest the formation of oxygen-containing functional groups on the surface of the GM foam. The calculated averaged relative atomic ratio of O to C as a function of UV/O_3 treatment time are reported in Fig. 2c; XPS data was collected randomly at 3 different positions on each exposure condition to estimate the error for each data point. It is interesting to note that even though the O/C ratio increases by more than a factor of two after a 60 sec UV-ozone exposure, that ratio is still relatively low at ~ 2%. We believe that the relatively low O/C ratio is due to the fact that the oxygen-contained functional groups are primarily generated on the surface of the graphene and CNTs. This may also be the reason why the XPS peaks associated with bonds such as C=O (at 287 eV) or HO–C=O (at 289 eV) are not detected. However, in this case, the low level of oxidation observed is actually beneficial, since our intent is to tailor the surface energy without sacrificing too much of the active material. The transmission electron microscopy (TEM) images of CNTs before and after UV-ozone treatment are shown in Fig. S2 to further confirmed the non-destructive nature of this improved functionality of carbon materials via UV-ozone process. IR spectra for the GM and UV-ozone treated GM foams were also acquired (Fig. 2d). It is clear that after UV/O_3 treatment a new peak develops at 1182 cm^{-1}, and the peak at 1740 cm^{-1} was enhanced, indicating the formation of carboxylic groups; the two peaks are attributed to the (C-O) and (C=O) stretching modes of carboxyl monomers, respectively, since carboxylic dimers display those modes at 1259 and 1713 cm^{-1} instead.[32-34] The same trends were observed in the IR spectra of SWCT after ozone treatment.[35] It should be noted that the GM foam already have some carboxyl group (dimer) on defect sites. The finding from the IR data is in accordance with the Raman spectra shown in Fig. 1c. The other peaks are assigned as listed in Table S1.

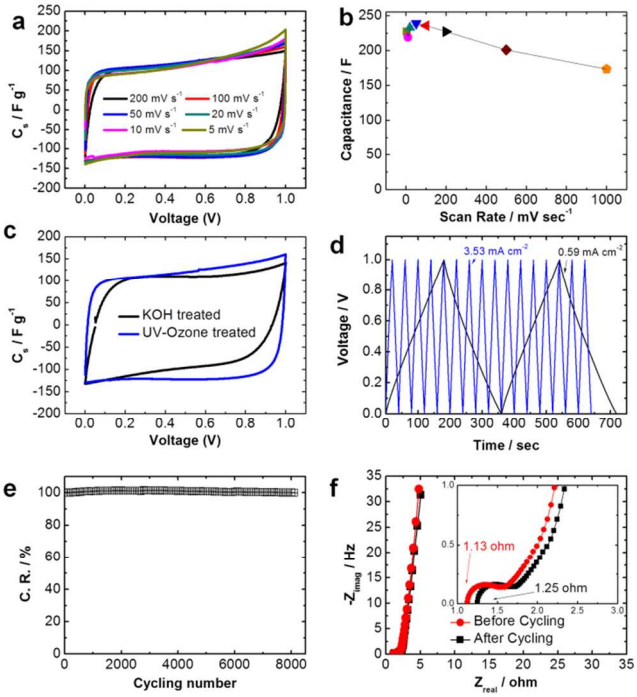

Fig. 3 (a) Normalized CV characteristics and (b) specific capacitances of UV-ozone treated GM foam under the scan rates of 5, 10, 20, 50, 100, 200 mV s^{-1}. (c) Comparison of CV characteristics of KOH treated GM foam and UV-ozone treated GM foam.[26] (d) Galvanostatic charge-discharge (CD) curves of GM SC at current densities of 0.59 mA cm^{-2} and 3.53 mA cm^{-2}, respectively. (e) Cycling stability test of UV-ozone treated GM foam at the current density of 56.5 mA cm^{-2}. (f) Potentiostatic electrochemical impedance spectroscopy (EIS) plots of UV-ozone treated GM foam before and after cycling test. Inset shows the high frequency region of the EIS plots.

SCs based on the UV Ozone treated (exposure time: 60 sec) GM nanostructure foam electrodes were fabricated, which include two equal area working electrodes spaced apart by a porous separator. Cyclic voltammetry (CV) for UV-ozone treated GM foam SC was initially conducted at scanning rates between 5

mV sec^{-1} and 200 mV sec^{-1} with an operational voltage window of 1 V in 2 M Li_2SO_4 aqueous electrolyte to estimate the capacitance. The nearly rectangular shape and the absence of oxidation and reduction peaks are observed for all scan rates suggesting that SCs based on UV-ozone GM electrodes have small equivalent series resistance, high rate capability, and excellent electrochemical performance. Moreover, the nearly mirror-image shape of CV curves indicate exceptional reversibility and a very fast surface reaction.[36] The nearly identical normalized CV characteristics for all scan rates <200 mV sec^{-1} suggest excellent process stability, repeatability, and outstanding performance of the SC based on UV-ozone treated GM foam. As shown in the specific capacitance against scan rates plot (Fig. 3b), the specific capacitance ~ 230 F g^{-1} was achieved for scan rates < 200 mV sec^{-1}. Specific capacitance retained is 80% for SC based on UV-ozone treated GM foam under a high scan rate of 1000 mV sec^{-1}, which is superior to that of pristine GM foam and GM foam with KOH treatment.[26] We believe there are two possible reasons leading to the excellent electrochemical performance of the UV-ozone treated GM SC system: (i) enhancement of electrode-electrolyte interface via UV-ozone treatment which increased the surface energy, and (ii) enhanced electrochemical stability of the innovative GM foam architecture.[37] Fig. 3c shows the normalized CV characteristics of KOH treated GM foam and UV-ozone treated GM foam. The UV-ozone treated GM shows sharper corners and more rectangular shape suggesting that SCs based on UV-ozone treated GM electrodes have faster current-voltage response, smaller equivalent series resistance, higher rate capability, and superior electrochemical performance. Chronopotentiometry measurements were also conducted with an operating voltage window of 1.0 V to further evaluate the electrochemical performance of the UV-ozone treated GM foam SCs. Charge-discharge (CD) characteristics demonstrate near linear and symmetric charge and discharge curves, suggesting an excellent capacitive performance with a rapid I-V response for our device (Fig. 3d). Cycling stability is another critical factor for the application of SC electrodes. A sequence of 8000 charge-discharge cycles for our UV-ozone treated GM nanostructure foam (Voltage window 1.0 V) was conducted under a current density of 56.5 mA cm^{-2} (Fig. 3e). A superior capacitance retention of 99% was maintained over 8000 cycles for the SC based on UV-ozone treated GM nanostructure.

Potentiostatic electrochemical impedance spectroscopy (EIS) measurements were performed to further characterize the performance of SCs based on GM and UV-ozone treated GM electrode. Both Nyquist plots (before and after cycling) show a linear and near vertical characteristic in the low frequency region, suggesting that the UV-ozone treated GM SC behaves approximately like an ideal capacitor.[38, 39] Some deviation from absolute ideality is evident in a large but finite slope of the plot in this region. This can be a result of frequency dispersion due to nonuniform distribution of the pore sizes in the porous matrix.[40] The near identical Nyquist plots and minor equivalent series resistance (ESR) change (from 1.13 to 1.25) for UV-ozone treated GM before and after cycling further verified the excellent electrochemical stability of our materials system (Fig. 3f).

Fig. 4a shows the equivalent circuit used to decipher the impedance plots obtained via EIS. This equivalent circuit is an electrical model whose elements represent individual electrochemical mechanisms inside the electric double layer capacitor (EDLC). To further study the effects of UV-ozone treatment on the electrochemical performance of GM based SCs, we compared the Nyquist plots for pristine GM,[26] KOH treated GM[26] and UV-ozone treated GM (Fig. 4b). The high frequency intercept is where the SC behaves like a pure resistor. This intercept, represented as R_S in the equivalent circuit, gives numerical information about ESR including the ionic resistance of electrolyte and electronic resistance in external contacts in the SC.[41] Lower values of R_S are desirable in order to achieve improved power performance from a SC. UVO treated GM demonstrates the lowest Rs~1.13 ohm compared with KOH treated GM (~1.54 ohm) and pristine GM (23.1 ohm). The semicircle in the high frequency region is due to contact impedance between the active material and the current collector.[17, 42] It may also signify contact resistance among active material particles, impedance between the active material and the current collector, etc.[43] A noticeable decrease of this semicircle in the high frequency region of the impedance plot is observed after applying both the UV-ozone treatment and KOH treatment. UVO treated GM foam shows the smallest semicircle, which only takes ~ 50% of the KOH treated GM SC (Fig. 4b inset). This provides evidence for improved contact among active material particles and with the current collector.

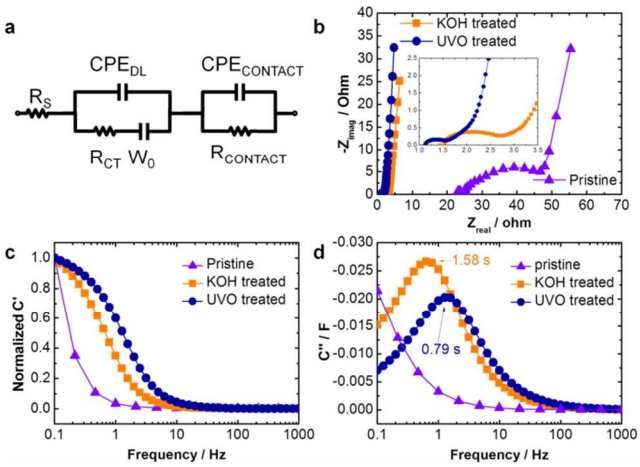

Fig. 4 (a) The equivalent circuit model used for EIS fitting, where R_S is the equivalent series resistance (*ESR*), R_{CT} is the resistance at the electrode-electrolyte interface, $R_{CONTACT}$ is the contact and interface resistance among active material and current collector. CPE_{DL} is the constant phase element (*CPE*) which represents non-ideal capacitance at the electrode-electrolyte interface, W_0 is the Warburg element representing diffusion impedance, and $CPE_{CONTACT}$ represents non-ideal capacitance at contact points among active material and current collector. Plots of (b) EIS spectra, (c) normalized real capacitances (C') versus frequency, and (d) imaginary capacitance versus frequency for pristine GM foam, KOH treated GM foam and UV-ozone treated GM foam, respectively.

The complex impedance plots provide evidence for an increased power capability in our SC after the ozone treatment. Normalized capacitance should stay fairly constant at 1 until

hitting characteristic frequency. A larger frequency region for which this stays true is desirable for SCs. In the Fig. below, an evident improvement in this stability is observed in the SC after Ozone treatment (Fig. 4c). The characteristic time constant can be derived from imaginary capacitance vs. frequency plot (Fig. 4d). It is a measure of how fast the device can be charged or discharged while maintaining good capacitive behavior.[17, 44, 45] It is observed that the UVO treated GM SC achieved the smallest characteristic time constant ~0.79 sec (highest corresponding characteristic frequency) which is a 100% improvement when compared against KOH treated GM foam (~1.58 sec) and much superior to pristine GM and other reported nanocarbon systems.[17, 44]

Conclusions

In summary, an improved functionality of carbon materials via a non-invasive high-throughput UV generated ozone (UV-ozone) treatment is achieved. We found that with the tuning of UV-ozone exposure time, the surface wettability of carbon nanostructure can be tailored transitionally. UV-ozone treatment leads the complete transition of graphene and CNT hybrid foam nanostructure (GM) from hydrophobic to hydrophilic in 60 sec. This simple and scalable process is verified to be non-invasive with excellent controllability. Symmetric SCs (SCs) based on the UV-ozone treated GM foam demonstrate enhanced rate performance. The results suggest this UV-ozone treatment method is a very promising dry processing approach to tailor carbonaceous electrodes for improved SC rate performance, durability, and stability. This technique can be readily applied to other CVD-grown carbonaceous materials by taking advantage of its processing ease, cost, scalability, and controllability.

Notes and references

[a] *Program of Materials Science and Engineering, Department of Mechanical Engineering, University of California, Riverside, CA, USA. E-mail: cozkan@engr.ucr.edu;*
[b] *Department of Electrical Engineering, University of California, Riverside, CA, USA. E-mail: mihri@ee.ucr.edu;*
[b] *Department of Chemistry, University of California, Riverside, CA, USA.*
** Corresponding author: mihri@ee.ucr.edu, cozkan@engr.ucr.edu*

† Electronic Supplementary Information (ESI) available: [details of any supplementary information available should be included here]. See DOI: 10.1039/b000000x/

Acknowledgement

I. L. and F. Z. acknowledge NSF grant DMR-0958796.

References

1. P. Simon and Y. Gogotsi, *Nature materials*, 2008, **7**, 845-854.
2. C. X. Guo and C. M. Li, *Energy & Environmental Science*, 2011, **4**, 4504-4507.
3. D. Pech, M. Brunet, H. Durou, P. Huang, V. Mochalin, Y. Gogotsi, P.-L. Taberna and P. Simon, *Nature nanotechnology*, 2010, **5**, 651-654.
4. L. L. Zhang and X. Zhao, *Chemical Society Reviews*, 2009, **38**, 2520-2531.
5. M. D. Stoller, S. Park, Y. Zhu, J. An and R. S. Ruoff, *Nano Letters*, 2008, **8**, 3498-3502.
6. Y. Zhu, S. Murali, M. D. Stoller, K. Ganesh, W. Cai, P. J. Ferreira, A. Pirkle, R. M. Wallace, K. A. Cychosz and M. Thommes, *Science*, 2011, **332**, 1537-1541.
7. A. B. Dalton, S. Collins, E. Munoz, J. M. Razal, V. H. Ebron, J. P. Ferraris, J. N. Coleman, B. G. Kim and R. H. Baughman, *Nature*, 2003, **423**, 703-703.
8. X. Lang, A. Hirata, T. Fujita and M. Chen, *Nature nanotechnology*, 2011, **6**, 232-236.
9. W. Wang, S. Guo, K. N. Bozhilov, D. Yan, M. Ozkan and C. S. Ozkan, *Small*, 2013, **9**, 3714-3721.
10. V. Augustyn, J. Come, M. A. Lowe, J. W. Kim, P.-L. Taberna, S. H. Tolbert, H. D. Abruña, P. Simon and B. Dunn, *Nature materials*, 2013, **12**, 518-522.
11. G. A. Snook, P. Kao and A. S. Best, *Journal of Power Sources*, 2011, **196**, 1-12.
12. K. Zhang, L. L. Zhang, X. Zhao and J. Wu, *Chemistry of Materials*, 2010, **22**, 1392-1401.
13. D. N. Futaba, K. Hata, T. Yamada, T. Hiraoka, Y. Hayamizu, Y. Kakudate, O. Tanaike, H. Hatori, M. Yumura and S. Iijima, *Nature materials*, 2006, **5**, 987-994.
14. W. Wang, S. Guo, M. Ozkan and C. S. Ozkan, *Journal of Materials Research*, 2013, **28**, 912-917.
15. J. Gamby, P. Taberna, P. Simon, J. Fauvarque and M. Chesneau, *Journal of Power Sources*, 2001, **101**, 109-116.
16. D.-D. Zhou, H.-J. Liu, Y.-G. Wang, C.-X. Wang and Y.-Y. Xia, *Journal of Materials Chemistry*, 2012, **22**, 1937-1943.
17. J. Chmiola, G. Yushin, R. Dash and Y. Gogotsi, *Journal of Power Sources*, 2006, **158**, 765-772.
18. M. F. El-Kady, V. Strong, S. Dubin and R. B. Kaner, *Science*, 2012, **335**, 1326-1330.
19. S. Guo, W. Wang, C. S. Ozkan and M. Ozkan, *Journal of Materials Research*, 2013, **28**, 918-926.
20. J. Chmiola, G. Yushin, Y. Gogotsi, C. Portet, P. Simon and P.-L. Taberna, *Science*, 2006, **313**, 1760-1763.
21. C. Largeot, C. Portet, J. Chmiola, P.-L. Taberna, Y. Gogotsi and P. Simon, *Journal of the American Chemical Society*, 2008, **130**, 2730-2731.
22. J. Lin, C. Zhang, Z. Yan, Y. Zhu, Z. Peng, R. H. Hauge, D. Natelson and J. M. Tour, *Nano Letters*, 2012, **13**, 72-78.
23. Z. Yan, L. Ma, Y. Zhu, I. Lahiri, M. G. Hahm, Z. Liu, S. Yang, C. Xiang, W. Lu and Z. Peng, *ACS nano*, 2012, **7**, 58-64.
24. Y. Zhu, L. Li, C. Zhang, G. Casillas, Z. Sun, Z. Yan, G. Ruan, Z. Peng, A.-R. O. Raji and C. Kittrell, *Nature communications*, 2012, **3**, 1225.
25. J. Lin, J. Zhong, D. Bao, J. Reiber-Kyle and W. Wang, *Journal of Nanoscience and Nanotechnology*, 2012, **12**, 1770-1775.
26. W. Wang, S. Guo, M. Penchev, I. Ruiz, K. N. Bozhilov, D. Yan, M. Ozkan and C. S. Ozkan, *Nano Energy*, 2013, **2**, 294-303.
27. X. Dong, Y. Ma, G. Zhu, Y. Huang, J. Wang, M. B. Chan-Park, L. Wang, W. Huang and P. Chen, *J. Mater. Chem.*, 2012, **22**, 17044-17048.
28. G. Zhu, Z. He, J. Chen, J. Zhao, X. Feng, Y. Ma, Q. Fan, L. Wang and W. Huang, *Nanoscale*, 2014, **6**, 1079-1085.
29. W. Wang, I. Ruiz, S. Guo, Z. Favors, H. H. Bay, M. Ozkan and C. S. Ozkan, *Nano Energy*, 2014, **3**, 113-118.
30. M. S. Dresselhaus, A. Jorio, M. Hofmann, G. Dresselhaus and R. Saito, *Nano letters*, 2010, **10**, 751-758.
31. J. Yuan, L.-P. Ma, S. Pei, J. Du, Y. Su, W. Ren and H.-M. Cheng, *ACS nano*, 2013, **7**, 4233-4241.
32. R. Nyquist, T. Clark and R. Streck, *Vibrational spectroscopy*, 1994, **7**, 275-286.
33. H. Naeimi, A. Mohajeri, L. Moradi and A. M. Rashidi, *Applied Surface Science*, 2009, **256**, 631-635.
34. J. Maillols, V. Tabacik and S. Sportouch, *Journal of Molecular Structure*, 1976, **32**, 173-190.
35. D. B. Mawhinney, V. Naumenko, A. Kuznetsova, J. T. Yates, J. Liu and R. Smalley, *Journal of the American Chemical Society*, 2000, **122**, 2383-2384.
36. Z. S. Wu, W. Ren, D. W. Wang, F. Li, B. Liu and H. M. Cheng, *ACS Nano*, 2010, **4**, 5835-5842.

37. W. Wang, S. R. Guo, K. N. Bozhilov, D. Yan, M. Ozkan and C. S. Ozkan, *Small*, 2013, **9**, 3714-3721.
38. A. K. Mishra and S. Ramaprabhu, *The Journal of Physical Chemistry C*, 2011, **115**, 14006-14013.
39. S. Buller, E. Karden, D. Kok and R. De Doncker, Modeling the dynamic behavior of supercapacitors using impedance spectroscopy, 2001.
40. H.-K. Song, H.-Y. Hwang, K.-H. Lee and L. H. Dao, *Electrochimica Acta*, 2000, **45**, 2241-2257.
41. B. Conway, V. Birss and J. Wojtowicz, *Journal of Power Sources*, 1997, **66**, 1-14.
42. C. Portet, P. Taberna, P. Simon and C. Laberty-Robert, *Electrochimica Acta*, 2004, **49**, 905-912.
43. Q. Cheng, J. Tang, J. Ma, H. Zhang, N. Shinya and L.-C. Qin, *Carbon*, 2011, **49**, 2917-2925.
44. C. Portet, P. L. Taberna, P. Simon, E. Flahaut and C. Laberty-Robert, *Electrochimica Acta*, 2005, **50**, 4174-4181.
45. M. Toupin, D. Bélanger, I. R. Hill and D. Quinn, *Journal of Power Sources*, 2005, **140**, 203-210.
46. J.-J. Max and C. Chapados, *The Journal of Physical Chemistry A*, 2004, **108**, 3324-3337.
47. E. Najafi, J.-Y. Kim, S.-H. Han and K. Shin, *Colloids and Surfaces A: Physicochemical and Engineering Aspects*, 2006, **284**, 373-378.
48. D. B. Mawhinney and J. T. Yates Jr, *Carbon*, 2001, **39**, 1167-1173.
49. H. Lewandowski, E. Koglin and R. J. Meier, *Vibrational spectroscopy*, 2005, **39**, 15-22.
50. S. Goyanes, G. Rubiolo, A. Salazar, A. Jimeno, M. Corcuera and I. Mondragon, *Diamond and related materials*, 2007, **16**, 412-417.
51. M. Burghard, *Surface Science Reports*, 2005, **58**, 1-109.
52. N. Qui, P. Scholz, T. Krech, T. Keller, K. Pollok and B. Ondruschka, *Catalysis Communications*, 2011, **12**, 464-469.

Cite this: DOI: 10.1039/c0xx00000x

www.rsc.org/xxxxxx

Communication